2026 RISP International Workshop on Nonlinear Circuits, Communications and Signal Processing
February 27 - March 2, 2026, Honolulu, Hawaii, U.S.A.

# Estimation of Functional Network Structure in iPSC-Derived Neural Signals Using Spatial Information

Yoko Uwate and Yoshifumi Nishio

Dept. of Electrical and Electronic Engineering, Tokushima University
2-1 Minami-Josanjima, Tokushima, Japan
Email: {uwate, nishio}@ee.tokushima-u.ac.jp

**Abstract**

This study proposes a method for estimating the network structure of human-derived iPS cell networks during their growth process. We focus on modularity as network metrics. We clarify how network topology evolves during this growth process.

## 1. Introduction

Understanding how neuronal networks develop synchronized activity is essential for revealing the principles of functional maturation in the brain. During early development, neuronal populations transition from irregular spiking to organized burst synchronization, reflecting the formation of functional connectivity [1], [2]. Human induced pluripotent stem cell (iPSC)-derived neuronal cultures have recently emerged as a powerful in vitro model for studying these developmental processes under controlled conditions, providing valuable insights into human-specific network dynamics [3], [4]. However, estimating functional network organization from large-scale neuronal activity recorded by multi-electrode arrays (MEAs) remains a challenging problem.

In this study, we propose a spatially informed method for estimating the functional network structure of iPSC-derived neuronal networks by integrating electrode position information with firing rate characteristics. Specifically, firing rate time series are computed for clustered electrodes and classified into multiple categories based on their firing activity. Functional connections are then constructed by preferentially linking spatially proximate electrodes with high firing rates. The proposed approach enables visualization of spatially localized high-activity regions and reveals functional organization embedded in the neuronal network. We focus on the modularity as network metrics. The number of communities is high in young cells and decreases with growth. At this stage, the network becomes a large network. As growth continues further, clustering of network nodes occurs again, and it was found that the number of communities increases. These results demonstrate that integrating neuronal activity signals with spatial information provides an effective framework for estimating functional network structure in iPSC-derived neuronal networks.

## 2. iPS Cell-Derived Networks

Human iPSC-derived neurons and astrocytes were plated on MaxWell chips [5], [6] at densities of 100,000 neurons and 20,000 astrocytes per chip. Chips were coated with polyethyleneimine (PEI) followed by laminin. Cells were maintained at 37°C, 5% $CO_2$, and 95% humidity. Electrophysiological recordings were performed at days in vitro (DIV) 11, 15, 19, 22, and 25. The recordings were performed using 1,024 electrodes at a sampling rate of 20 kHz. Experiments were conducted on three separate plates (Pl1, Pl2, and Pl3).

Neural activity is recorded using 1024 electrodes, but in this study, cluster electrodes are detected as typical electrodes (which is named cluster electrode). Cluster electrode detection was performed based on electrode spatial coordinates. Electrodes with observed spikes were considered valid, and their coordinates were used to construct a KD-tree for efficient spatial querying. For each unvisited electrode, all neighboring electrodes within a radius of 100 μm were identified and grouped into a cluster. The cluster center was defined as the centroid of the member electrode coordinates, and a representative electrode for the cluster was chosen as the electrode closest to the centroid.

The results of the selected cluster electrodes are shown in Fig. 1. It can be seen that the main electrodes were chosen from neighboring electrodes. As a result, the 1,024 electrodes can be reduced to approximately 70 main electrodes.

To characterize the developmental changes in neuronal activity, we analyzed the firing-rate distribution of cluster electrodes at DIV11, DIV15, DIV19, DIV22, and DIV25. Spike times were extracted from the recorded spike trains and converted to firing rates by dividing the total number of spikes by the recording duration (60 s) for each cluster electrode. The firing rates were classified into five categories using fixed thresholds: Very low (0–1 Hz), Low (1–2 Hz), Medium (2–3

Hz), High (3–4 Hz), and Very high (4–5 Hz).

Figure 2 shows the firing-rate histograms of cluster electrodes at different developmental stages (DIV11–DIV25). At earlier stages (DIV11 and DIV15), most cluster electrodes fall into the Very low and Low firing-rate categories, indicating predominantly sparse spontaneous activity. With development (DIV19–DIV25), the distribution gradually shifts, showing an increased proportion of Medium and higher firing-rate categories. These results indicate a developmental change in the overall firing-rate distribution, providing a quantitative overview of activity maturation across DIVs.

Figure 3 shows raster plots of the cluster electrodes at different DIVs. The colors of the spike columns correspond to the firing frequency categories determined above. Even if the number of electrodes decrease, the main behavior of spike activities can be confirmed.

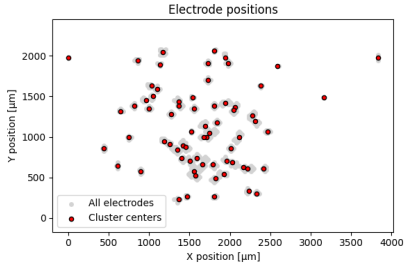


Figure 1: Cluster Electrodes.

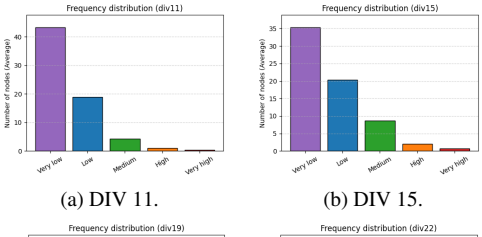


(a) DIV 11. (b) DIV 15.

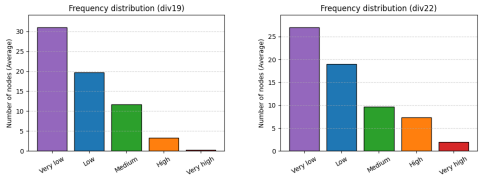


(c) DIV 19. (d) DIV 22.

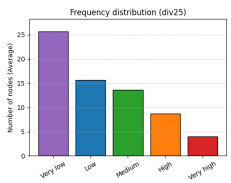


(e) DIV 25.

Figure 2: Histogram of Firing Rate.

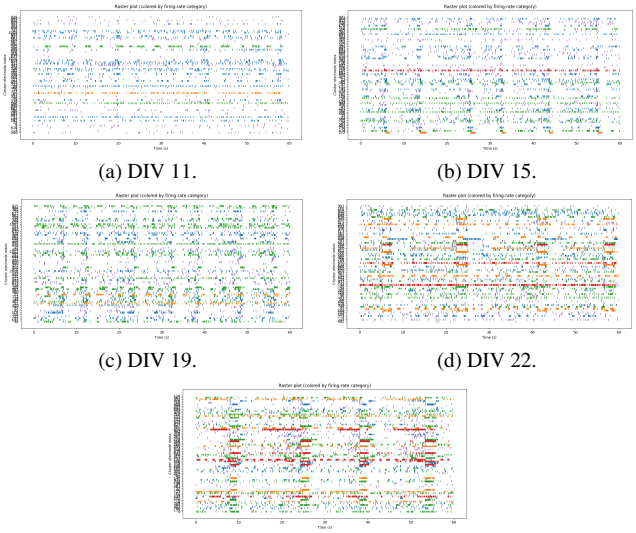

(a) DIV 11. (b) DIV 15.

(c) DIV 19. (d) DIV 22.

(e) DIV 25.

Figure 3: Raster Plots of Cluster Electrodes.

## 2.1 Network Construction Based on Firing Rates

A functional network was constructed by assigning a node-specific number of connections based on neuronal firing rates. Let $r_i$ denote the firing rate of node $i$. The firing rates were first normalized as

$$\tilde{r}_i = \frac{r_i - r_{\min}}{r_{\max} - r_{\min}}, \tag{1}$$

where $r_{\min}$ and $r_{\max}$ represent the minimum and maximum firing rates across all nodes, respectively.

The number of connections $k_i$ assigned to node $i$ was then determined using a power-law scaling:

$$k_i = \lfloor k_{\min} + (k_{\max} - k_{\min})\tilde{r}_i^{\alpha} \rfloor, \tag{2}$$

where $k_{\min} = 1$ and $k_{\max} = 10$ denote the minimum and maximum allowable number of connections, $\alpha = 2$ is the scaling exponent, and $\lfloor \cdot \rfloor$ indicates the floor function.

To establish network edges, the Euclidean distance between nodes $i$ and $j$ was computed as

$$d_{ij} = \|\mathbf{x}_i - \mathbf{x}_j\|, \tag{3}$$

where $\mathbf{x}_i$ represents the spatial coordinates of node $i$. For each node, connections were sequentially formed with the nearest unconnected nodes until the prescribed number of connections $k_i$ was reached. Duplicate edges were avoided, resulting in an undirected network.

This construction ensures that nodes with higher firing rates tend to have a larger number of connections while preserving spatial locality.

## 3. Simulation Results

Figure 4 shows the networks constructed using the proposed method at different developmental stages. At DIV11, the network is sparse with a small number of edges. As development progresses, the number of highly active neurons increases, leading to a gradual increase in network connectivity. At DIV15, most nodes form a single connected component, giving rise to a globally integrated network structure. In contrast, at DIV25, the network exhibits renewed clustering, indicating the emergence of modular organization.

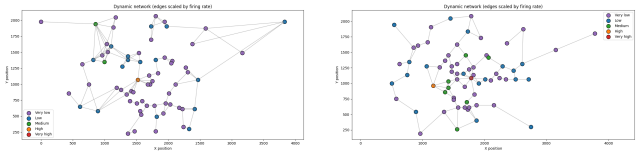

(a) DIV 11.



(b) DIV 15.

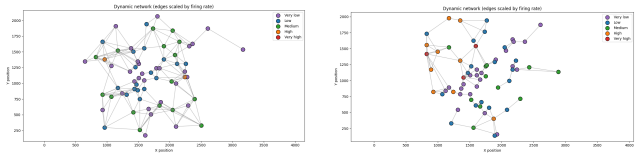

(c) DIV 19.



(d) DIV 22.

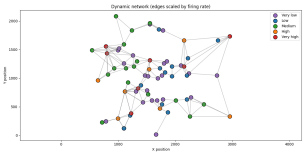

(e) DIV 25.

Figure 4: Network Construction (Pl1).

Next, Figure 5 presents the averages of the total number of edges and the clustering coefficient, calculated across Pl1–Pl3, as global network metrics. Consistent with the qualitative network evolution described above, the total number of edges initially increases during development and then shows a decreasing trend at later stages. In contrast, the clustering coefficient remains relatively high and stable after div15, suggesting the persistence of locally clustered structures despite changes in overall connectivity.

### 3.1 Modularity Analysis

To quantify the community structure of the estimated networks, we evaluated the network modularity $Q$. Modularity measures the extent to which a network can be partitioned into densely connected communities with sparse connections between them.

Finally, modularity was computed using a graph-based community detection algorithm implemented in the NetworkX library, which identifies communities by maximizing

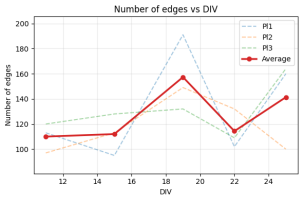


(a) Average Number of Edges.

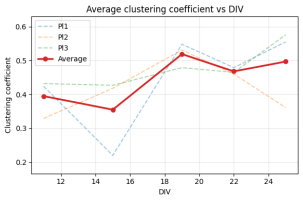


(b) Average Clustering Coefficient.

Figure 5: Network Characteristics.

the modularity score. The modularity $Q$ is defined as

$$Q = \frac{1}{2m} \sum_{i,j} \left( A_{ij} - \frac{k_i k_j}{2m} \right) \delta(c_i, c_j), \tag{4}$$

where $A_{ij}$ represents the adjacency matrix of the network, $k_i$ and $k_j$ denote the degrees of nodes $i$ and $j$, respectively, $m$ is the total number of edges, and $\delta(c_i, c_j)$ is an indicator function that equals 1 if nodes $i$ and $j$ belong to the same community and 0 otherwise.

A higher modularity value indicates a stronger community structure, meaning that nodes are more densely connected within communities than expected in a random network with the same degree distribution. Conversely, lower modularity values suggest a more homogeneous or globally integrated network organization.

Figure 6 shows the simulation result of average of modularities (Pl1–Pl3). We observed that the modularity $Q$ changed non-monotonically across developmental stages. Specifically, modularity decreased at intermediate stages and subsequently increased at later stages, indicating a transient reduction followed by a re-emergence of community structure during network development.

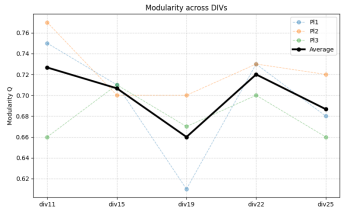


Figure 6: Average Network Modularity.

Figure 7 shows the network community structures identified by modularity optimization. At DIV11, the network is divided into ten communities. The number of communities decreases to five at DIV19, whereas at DIV25 the network is again separated into eight communities, reflecting dynamic changes in community organization during development.

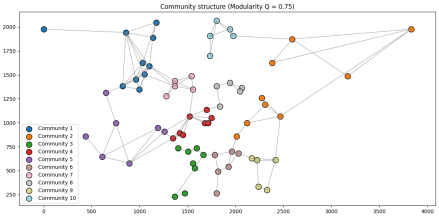


(a) DIV11.

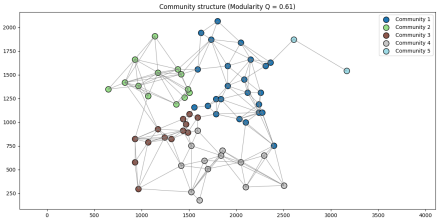


(b) DIV19.

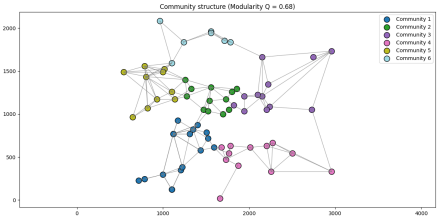


(c) DIV25.

Figure 7: Network Modurality (Pl1).

## 4. Conclusion

In this study, we investigated the developmental changes in neuronal network structures reconstructed from multi-electrode array recordings. Cluster electrodes were first identified based on spatial proximity, and their firing rates were quantified and categorized into five levels. Using a distance-constrained network construction method in which the number of connections per node was nonlinearly scaled according to firing rate, we reconstructed spatial networks at different developmental stages.

The results demonstrated that both network topology and community structure dynamically changed during development. At early stages, the networks exhibited sparse connectivity and a relatively large number of communities. At intermediate stages, the network became more integrated, accompanied by an increase in edge density and a reduction in the number of communities. At later stages, the network showed reorganization characterized by increased modularity and re-emergence of community structures.

These observations suggest that the spatial and functional organization of neuronal networks evolves non-monotonically during development. The proposed framework provides a systematic approach to linking firing activity, spatial constraints, and network topology, and may be useful for characterizing developmental dynamics in in vitro neuronal networks.

## Acknowledgment

The authors would like to thank MaxWell Biosystems for providing the iPSC-derived neuronal recording data used in this study. This work was partly supported by JSPS KAKENHI Grant Number JP25K15273.

## References

[1] P. J. Uhlhaas, F. Roux, E. Rodriguez, A. Rotarska-Jagiela, W. Singer, “Neural Synchrony and the Development of Cortical Networks” *Trends in Cognitive Sciences*, Vol.14 No.2, pp. 72–80, Feb. 2010.

[2] H. J. Luhmann, A. Sinning, J-W. Yang, V. Reyes-Puerta, M. C. Stüttgen, S. Kirischuk, W. Kilb, “Spontaneous Neuronal Activity in Developing Neocortical Networks: From Single Cells to Large-Scale Interactions,” *Front. Neural Circuits*, Vol. 10, pp. 820-837, May 2016.

[3] A. M. Tukker, F. M.J. Wijnolts, A. de Groot, R. H.S. Westerink, “Human iPSC-Derived Neuronal Models for in vitro Neurotoxicity Assessment,” *NeuroToxicology*, Vol. 67, pp. 215–225, Jul. 2018.

[4] K. Bartmann, F. Bendt, A. Dönmez, D. Haag, E. Kessel, S. Masjosthusmann, C. Noel, J. Wu, P. Zhou, E. Fritsche, “A Buman iPSC-Based in vitro Neural Network Formation Assay to Investigate Neurodevelopmental Toxicity of Pesticides,” *bioRxiv*, doi: https://doi.org/10.1101/2023.01.12.523741, Jan. 2023.

[5] U. Frey, J. Sedivy, F.Heer, R. Pedron,M.Ballini, J. Mueller and A.Hierlemann, “Switch-Matrix-Based HighDensity Microelectrode Array in CMOS Technology,” *IEEE Solid-State Circuits*, 45(2), 467482. http://doi.org/10.1109/JSSC.2009.2035196, 2010.

[6] D. J. Bakkum U. Frey, M. Radivojevic, T. L. Russell, J. Mller, M. Fiscella and A. Hierlemann, “Tracking Axonal Action Potential Propagation on a High-Density Microelectrode Array Across Hundreds of Sites,” *Nature Communications*, 4, 2181. http://doi.org/10.1038/ncomms3181, 2013.